nature biomedical engineering

ARTICLES

https://doi.org/10.1038/s41551-019-0508-y

Glucose-responsive insulin patch for the regulation of blood glucose in mice and minipigs

Jicheng Yu[1,2], Jinqiang Wang[1,3,4], Yuqi Zhang[1,2], Guojun Chen[1,3,4], Weiwei Mao[2], Yanqi Ye[1,2], Anna R. Kahkoska[5], John B. Buse[5], Robert Langer[6,7,8,9,10] and Zhen Gu[1,3,4,11,12]*

Glucose-responsive insulin delivery systems that mimic pancreatic endocrine function could enhance health and improve quality of life for people with type 1 and type 2 diabetes with reduced β-cell function. However, insulin delivery systems with rapid in vivo glucose-responsive behaviour typically have limited insulin-loading capacities and cannot be manufactured easily. Here, we show that a single removable transdermal patch, bearing microneedles loaded with insulin and a non-degradable glucose-responsive polymeric matrix, and fabricated via in situ photopolymerization, regulated blood glucose in insulin-deficient diabetic mice and minipigs (for minipigs >25 kg, glucose regulation lasted >20 h with patches of ~5 cm²). Under hyperglycaemic conditions, phenylboronic acid units within the polymeric matrix reversibly form glucose–boronate complexes that—owing to their increased negative charge—induce the swelling of the polymeric matrix and weaken the electrostatic interactions between the negatively charged insulin and polymers, promoting the rapid release of insulin. This proof-of-concept demonstration may aid the development of other translational stimuli-responsive microneedle patches for drug delivery.

Diabetes—a chronic disease that often leads to severe secondary complications—affects over 425 million people around the world[1,2]. Insulin therapy is required for life in the setting of type 1 diabetes and is often used in type 2 diabetes with reduced islet β-cell function. It generally involves frequent monitoring of blood glucose levels and multiple subcutaneous injections daily or infusion to allow dose adjustment for safety and efficacy[1,3]. However, such treatment strategies are burdensome and often complicated by inadequate control and life-threatening hypoglycaemia resulting from miscalculated dose.

An effective glucose-responsive system, in which blood glucose monitoring information and insulin delivery are linked and occur without the patient's involvement, would release insulin in response to elevated glucose concentrations and regulate glucose levels within a normal range, with a reduced risk of hypoglycaemia[4–7]. To this end, artificial pancreas-like closed-loop insulin delivery systems are being developed to intelligently mimic the pancreatic endocrine functions for self-regulated insulin delivery[4–6]. Among them, glucose oxidase[8–13], glucose-binding protein[14–17] and phenylboronic acid (PBA)[18–23] are widely utilized as glucose-sensing elements to display glucose-dependent insulin release. Nonetheless, challenges remain to demonstrate a formulation or device for glucose-responsive insulin delivery that would combine desired features including: (1) rapid in vivo glucose-responsive behaviour with similar pharmacokinetics to pancreatic β-cells; (2) sufficient insulin-loading capacity for daily usage; (3) small size and/or simple design for ease of administration; (4) feasibility for large-scale manufacturing; and (5) high biocompatibility without acute and long-term toxicity[1,8,24]. Here, we present a strategy to easily create a coin-sized transdermal smart insulin patch (Fig. 1) that achieves a clinically relevant dose and fast glucose-dependent insulin release, as demonstrated in a minipig model (>25 kg) with insulin-deficient diabetes.

In this glucose-responsive microneedle (GR-MN) patch, the entire polymeric matrix of needles associated with PBA serves as the glucose-responsive component. Importantly, to obtain sufficient insulin-loading capacity for clinical use, this polymeric matrix of poly(*N*-vinylpyrrolidone-*co*-2-(dimethylamino)ethyl acrylate-*co*-3-(acrylamido)PBA) is formed through a convenient in situ photopolymerization method with a mixture of insulin, monomers and crosslinker (ethylene glycol dimethacrylate (EGDMA)) (Fig. 1a). PBA can reversibly interact with glucose to generate cyclic boronate esters, which shifts the equilibrium to the negatively charged groups[25–28]. When exposed to hyperglycaemic conditions, the reversible formation of a glucose–boronate complex in the 3-(acrylamido)PBA (3APBA) units results in an increase of negative charges within the polymeric matrix and leads to enhanced swelling of the microneedle, triggering rapid diffusion of the preloaded insulin into the skin tissue (Fig. 1b). At the same time, the increased density of negative charges also weakens the electrostatic interaction between the positively charged (dimethylamino)ethyl acrylate (DMAEA) units and the negatively charged insulin molecules, further promoting the release of insulin. Under normoglycaemic conditions, the inhibited volume variation and the restore of electrostatic interaction slow the insulin release rates, reducing the risk of hypoglycaemia. We demonstrate that GR-MN patches with a size of ~5 cm² were able to effectively regulate plasma glucose levels (PGLs) with rapid responsiveness in streptozotocin (STZ)-induced diabetic minipigs for over 20 h.

[1]Joint Department of Biomedical Engineering, University of North Carolina at Chapel Hill and North Carolina State University, Raleigh, NC, USA. [2]Zenomics Inc., Los Angeles, CA, USA. [3]Department of Bioengineering, University of California, Los Angeles, Los Angeles, CA, USA. [4]California NanoSystems Institute, University of California, Los Angeles, Los Angeles, CA, USA. [5]Department of Medicine, University of North Carolina School of Medicine, Chapel Hill, NC, USA. [6]Department of Chemical Engineering, Massachusetts Institute of Technology, Cambridge, MA, USA. [7]David H. Koch Institute for Integrative Cancer Research, Massachusetts Institute of Technology, Cambridge, MA, USA. [8]Department of Anesthesiology, Boston Children's Hospital, Boston, MA, USA. [9]Division of Health Science and Technology, Massachusetts Institute of Technology, Cambridge, MA, USA. [10]Institute for Medical Engineering and Science, Massachusetts Institute of Technology, Cambridge, MA, USA. [11]Jonsson Comprehensive Cancer Center, University of California, Los Angeles, Los Angeles, CA, USA. [12]Center for Minimally Invasive Therapeutics, University of California, Los Angeles, Los Angeles, CA, USA. *e-mail: guzhen@ucla.edu

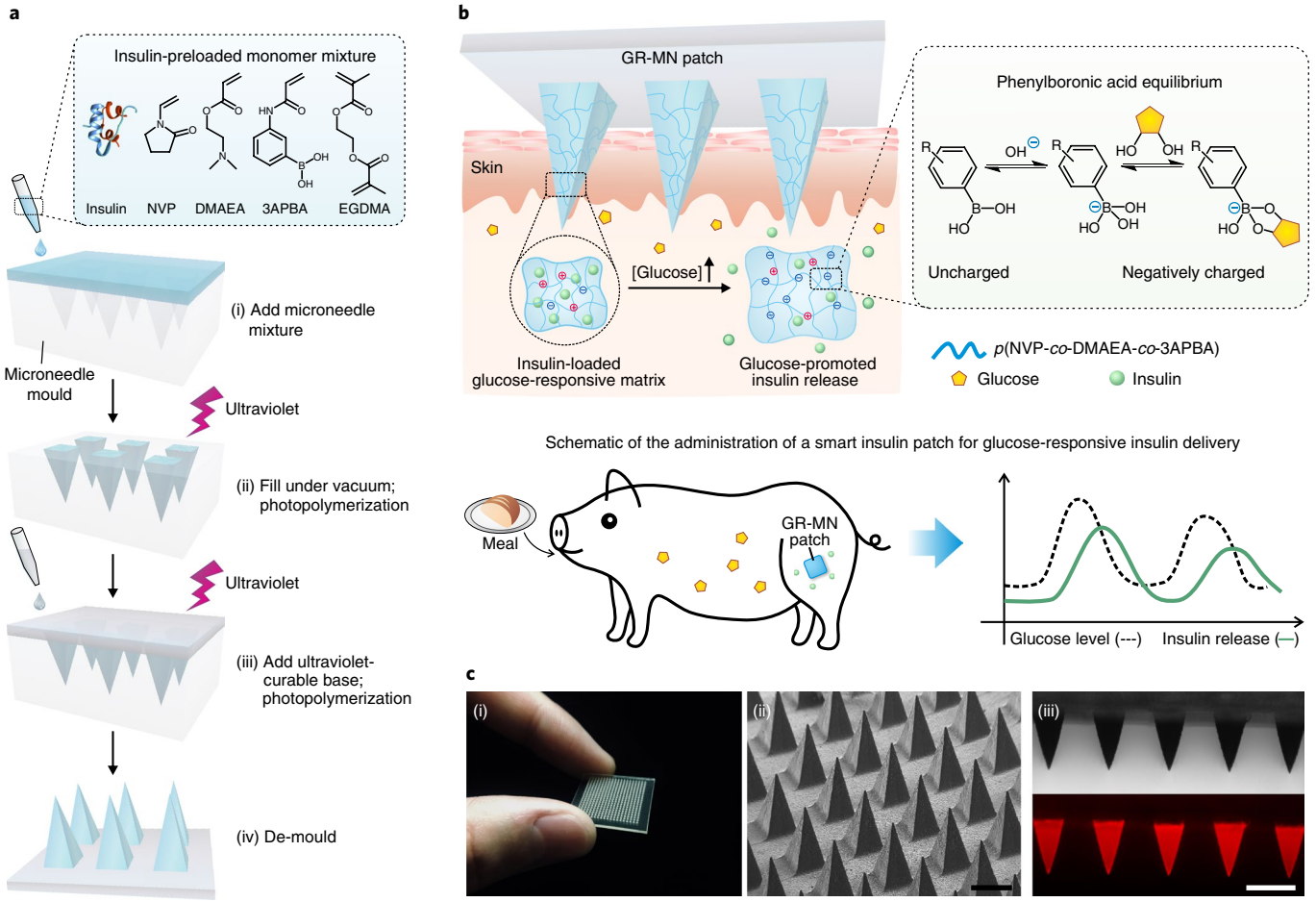

Fig. 1 | Schematic of the glucose-responsive insulin delivery system using microneedle-array patches with glucose-responsive matrix. a, Schematic of the fabrication process of a glucose-responsive insulin patch from a silicone mould using an in situ photopolymerization strategy. **b**, Mechanism of glucose-triggered insulin release from GR-MNs. Upon exposure to a hyperglycaemic state, the increased negative charges resulting from the formation of the glucose–boronate complexes can weaken the electrostatic interaction between negatively charged insulin and polymers and induce the volume variation of polymeric matrix, promoting the quick release of insulin from the microneedles. Glucose levels of diabetic pigs can be effectively regulated by the administration of a glucose-responsive insulin patch. **c**, Characterization of the GR-MN. (i) Photograph of the GR-MN patch. (ii) Scanning electron microscopy image of the microneedle array. Scale bar, 500 μm. (iii) Microscopy (top) and fluorescence microscopy (bottom) images of the rhodamine B-labelled insulin (red)-loaded microneedle patch. Scale bar, 500 μm.

Preparation and characterization of the GR-MN patch

The needles of the GR-MN patch are comprised of insulin-loaded glucose-responsive polymeric matrix, which is fabricated from an insulin-preloaded monomer mixture of *N*-vinylpyrrolidone (NVP), DMAEA, 3APBA and EGDMA by in situ photopolymerization at 4 °C (Fig. 1a). The NVP was chosen as the major monomer since it is liquid under ambient conditions[29,30] and can therefore act as a solvent to dissolve other monomers. A sample of the microneedle patch in Fig. 1c was arranged in a 20 × 20 array; each needle had a pyramidal shape, with a width of 400 μm at the base and a height of 900 μm. Afterwards, the base of the patch was further prepared using a flexible commercial ultraviolet-curable material. The sizes of patches used in the following animal studies were adjusted to tune the dosages of insulin. To reduce the residual monomers, the resulting patches were immersed in phosphate buffered saline (PBS)/ethanol mixtures (80:20; *v*/*v*) for 2 h. The amounts of leachable unreacted monomers from the purified microneedles were measured by high-performance liquid chromatography (HPLC) (Supplementary Table 1). The total weight of residual monomers was <0.5% of the entire patch and did not exceed the safety limits defined in the current toxicity database (https://pubchem.ncbi.nlm.nih.gov/). The fluorescence image of the GR-MN patch revealed that rhodamine B-labelled insulin was uniformly distributed in the entire polymeric matrix of each needle (Fig. 1c). In addition, the in situ photopolymerization method led to an encapsulation efficiency of insulin of 100% with a high loading capability of 20 wt% for microneedles. Although 9.9 ± 1.1% of insulin was released from the patch during the purification process, the resulting formulation was able to meet the target for potential clinical usage. We further determined the fracture force of the microneedle to be 0.90 ± 0.35 N per needle using a tensile compression machine (Fig. 2a), which is sufficient for skin penetration without breaking[8,31].

During the fabrication of microneedle patches, avoidance of extra organic solvent and elevated temperature was required to maintain the stability of insulin. The insulin extracted from the resulting patches exhibited a similar hypoglycaemic effect as freshly dissolved human recombinant insulin in diabetic mice (Fig. 2b). Mass spectrum analysis of the native insulin and the insulin extracted from the patch further confirmed that the insulin molecule was intact after the polymerization process (Supplementary Fig. 1). In addition, the polymeric microneedle could prevent denaturation of the loaded insulin at room temperature. By comparing the extracted insulin from the patches stored at room temperature with the freshly dissolved human recombinant insulin solution, we estimated that the

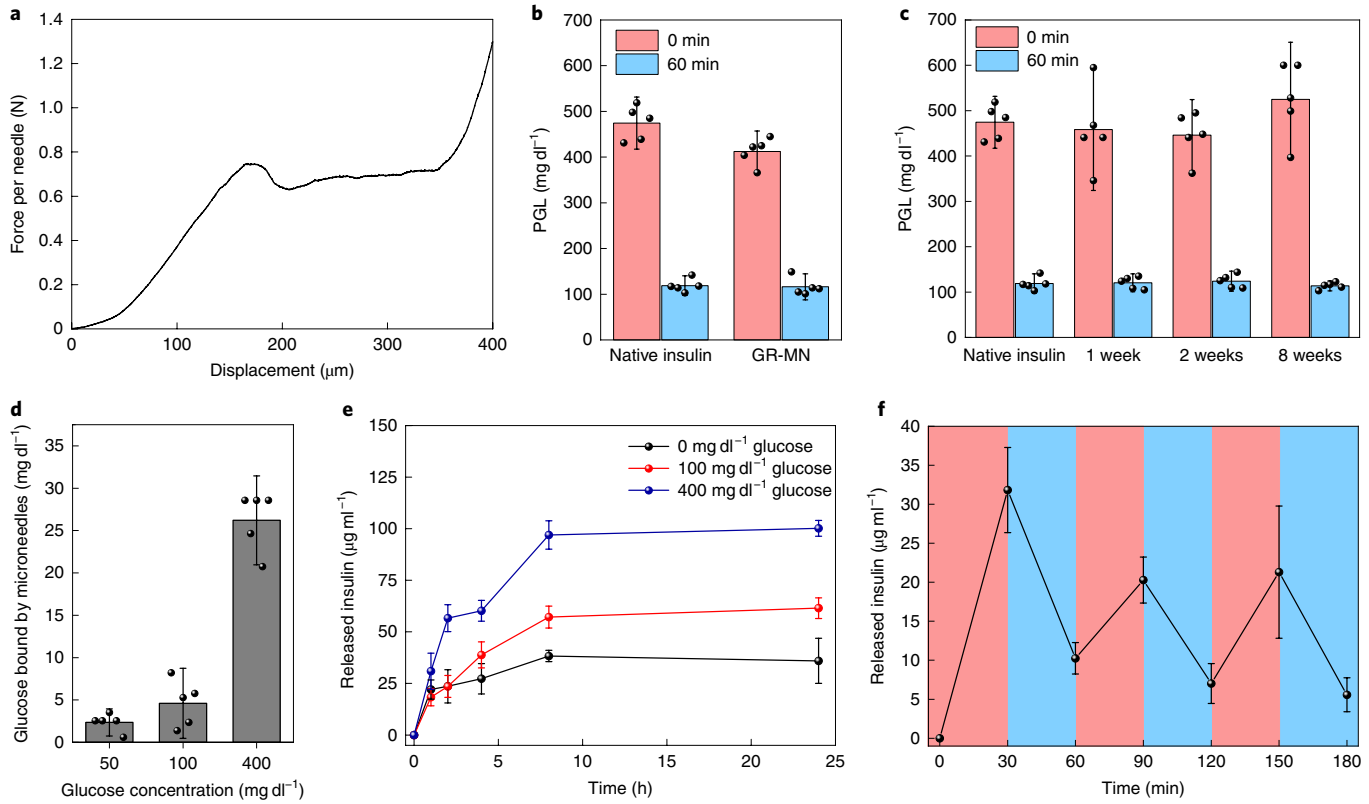

Fig. 2 | Characterization of the GR-MN. a, Mechanical behaviour of the GR-MNs. **b**, Glucose-lowering activity of the insulin extracted from the freshly prepared patch in diabetic mice ($n=5$). Initial glucose levels were compared with glucose levels at 60 min post-injection of insulin solution. **c**, Glucose-lowering activity of the insulin extracted from the patches stored at room temperature in diabetic mice ($n=5$). **d**, Glucose concentration-dependent glucose-binding capability of the glucose-responsive polymeric matrix ($n=3$). **e**, In vitro accumulated insulin release of the glucose-responsive polymeric matrix ($n=3$) in several glucose concentrations at 37 °C. **f**, Pulsatile release profile showing the rate of insulin release from the glucose-responsive polymeric matrix ($n=3$) as a function of the glucose concentration (blue: 100 mg dl^{-1}; red: 400 mg dl^{-1}). In **b**–**f**, data are presented as mean ± s.d.

stability of insulin within the patch could be maintained at room temperature for at least 8 weeks (Fig. 2c).

In vitro glucose-responsive insulin release

The PBA group has been used previously for the detection of glucose. An essential parameter for its selective binding to glucose is the pK_a of the PBA group[19,27,32]. To decrease the pK_a of 3APBA to enhance its glucose recognition capability at physiological pH, the Lewis base DMAEA was introduced to stabilize the borate ester by establishing electrostatic attraction (B^-–N^+) through protonated dimethylamino groups[26,28,33,34]. The glucose-binding capability of the resulting polymeric matrix with a 1:4 ratio of DMAEA to 3APBA was measured by incubation in PBS with varying glucose concentrations. The quantity of glucose bound by the polymeric matrix in a typical hyperglycaemic state (400 mg dl^{-1}) was 5.7-fold greater than that bound in a normoglycaemic state (100 mg dl^{-1}) (Fig. 2d).

The enhanced glucose binding under hyperglycaemic conditions led to an increased density of negative charges within the polymeric matrix, causing the volume variation and weakening the electrostatic interaction between insulin and the matrix. As shown in Supplementary Fig. 2, the solid GR-MNs displayed obvious swelling once exposed to a hyperglycaemic level for 1 h. In contrast, the GR-MNs demonstrated minimal change when incubated in saline or solution with a normal glucose concentration. The release rates of insulin were studied across samples with different ratios of the positively charged unit (DMAEA) to the negatively charged unit (3APBA). In the polymeric matrix with a 1:4 ratio of DMAEA to 3APBA, quick release of insulin was observed at the 400 mg dl^{-1} glucose level while a relatively slow release occurred at the 0 and 100 mg dl^{-1} glucose levels (Fig. 2e). In contrast, the release rates of insulin across all glucose concentrations were slow in the samples with a 1:1 ratio of DMAEA to 3APBA and the release rates were fast in the samples with a 1:20 ratio of DMAEA to 3APBA, which can be attributed to the excess positive or negative charges within the matrix (Supplementary Fig. 3). The rapid release of insulin from the polymeric matrix, due to the charge switch of insulin from negative to positive under acidic conditions or increased negative charges of 3APBA under basic conditions, further confirmed that electrostatic interaction plays an important role in the regulation of insulin release (Supplementary Fig. 4). The glucose-responsive release rates can be further tuned to satisfy the clinical needs of different populations by slightly adjusting the ratio of DMAEA to 3APBA. In the polymeric matrix with a 1:3 or 1:5 ratio of DMAEA to 3APBA, the release rates of insulin from the polymeric matrix at the hyperglycaemic state and the normoglycaemic state displayed different profiles compared with the sample with a 1:4 ratio (Supplementary Fig. 5). In addition, at the 1:4 ratio of DMAEA to 3ABPA, the rate of insulin release increased as glucose concentrations were gradually increased from normoglycaemic to hyperglycaemic conditions (Supplementary Fig. 6). A pulsatile release profile of insulin was also achieved for several cycles by incubating the polymeric matrix in the normal and hyperglycaemic solutions alternately (Fig. 2f). Taken together, the results substantiated that the release rate of insulin from the polymeric matrix was regulated in a glucose-dependent manner.

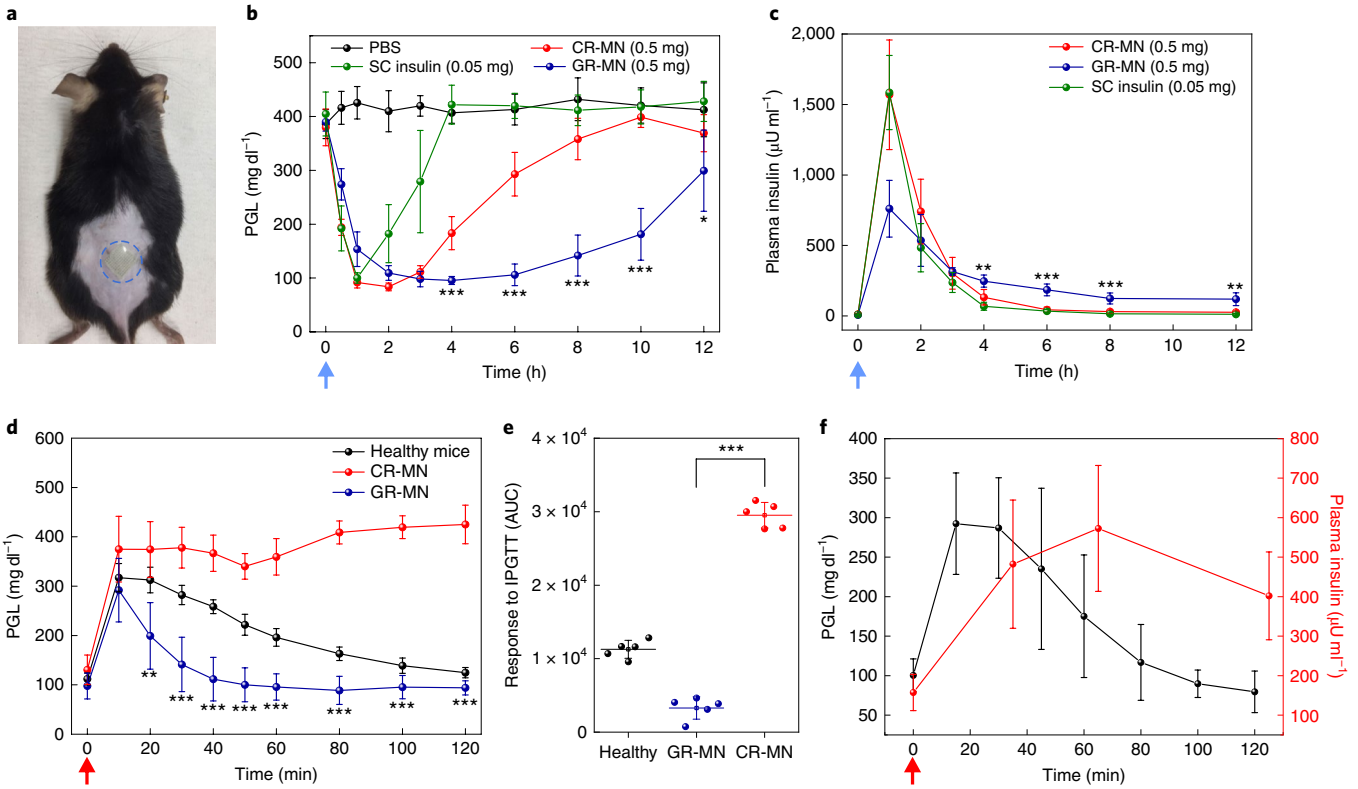

Fig. 3 | In vivo evaluation of the GR-MN patch in an STZ-induced diabetic mouse model. a, Mouse dorsum skin (the area within the blue dashed line) transcutaneously treated with a microneedle patch. **b**,**c**, PGLs (**b**) and plasma human insulin concentrations (**c**) in STZ-induced diabetic mice ($n=5$) after treatment with PBS, subcutaneous insulin solution (insulin dose: 0.05 mg), the CR-MN patch (insulin dose: 0.5 mg) or the GR-MN patch (insulin dose: 0.5 mg). SC, subcutaneous. Statistical significance for comparison of the GR-MN and CR-MN groups was determined by two-tailed Student's *t*-test (from left to right in **b**: $^{***}P=2.94\times10^{-4}$ at 4 h; $^{***}P=1.29\times10^{-5}$ at 6 h; $^{***}P=1.16\times10^{-5}$ at 8 h; $^{***}P=1.09\times10^{-5}$ at 10 h; $^{*}P=0.0478$ at 12 h; from left to right in **c**: $^{**}P=6.42\times10^{-3}$ at 4 h; $^{***}P=1.21\times10^{-4}$ at 6 h; $^{***}P=9.45\times10^{-4}$ at 8 h; $^{**}P=2.14\times10^{-3}$ at 12 h). **d**, In vivo intraperitoneal glucose tolerance test in diabetic mice ($n=5$) at 4 h post-administration of GR-MN or CR-MN compared with healthy control mice. Glucose dose: 1.5 g kg^{-1}. Statistical significance for comparison of the GR-MN and CR-MN groups was determined by two-tailed Student's *t*-test ($^{**}P=2.13\times10^{-3}$ at 20 min; $^{***}P=5.76\times10^{-5}$ at 30 min; $^{***}P=8.89\times10^{-6}$ at 40 min; $^{***}P=1.64\times10^{-6}$ at 50 min; $^{***}P=1.18\times10^{-6}$ at 60 min; $^{***}P=5.06\times10^{-8}$ at 80 min; $^{***}P=1.96\times10^{-8}$ at 100 min; $^{***}P=1.02\times10^{-7}$ at 120 min). **e**, Responsiveness in diabetic mice ($n=5$) was calculated based on the area under the curve (AUC) from 0–120 min, with the baseline set at the 0-min plasma glucose reading. Statistical significance was determined by two-tailed Student's *t*-test ($^{***}P=6.26\times10^{-9}$). **f**, In vivo glucose-responsive insulin release promoted by intraperitoneal glucose challenge at 4 h post-administration of GR-MN in diabetic mice ($n=5$). Glucose dose: 3 g kg^{-1}. In **b**,**c**, the blue arrows indicate the time points of microneedle administration. In **d**,**f**, the red arrows indicate the time points of glucose administration. In **b**–**f**, data are presented as mean ± s.d.

In vivo studies in an STZ-induced diabetic mouse model

We assessed the in vivo performance of the GR-MN with a 1:4 ratio of DMAEA to 3ABPA in an STZ-induced insulin-deficient diabetic mouse model. Diabetic mice were randomly grouped and transcutaneously exposed to either GR-MN patches or non-responsive crosslinked microneedle (CR-MN) patches as a control (insulin dose: 0.5 mg) (Fig. 3a). The PGLs of treated mice were monitored over time. As expected, the PGLs in mice treated with CR-MN and GR-MN patches all decreased to below 200 mg dl^{-1} (Fig. 3b). However, the normoglycaemic state could not be maintained in the groups treated with CR-MNs, and the glucose levels returned to a hyperglycaemic state after 4 h. In contrast, the GR-MN patch was shown to regulate glucose levels within the target range (<200 mg dl^{-1}) for more than 10 h. Plasma insulin measurement by an enzyme-linked immunosorbent assay (ELISA) displayed a continuous insulin release in the GR-MN group, consistent with sustained euglycaemic levels (Fig. 3c). The relative bioavailability (RBA) of the GR-MN patch was determined to be 11.6 ± 1.9% compared with subcutaneous injection of insulin (Supplementary Table 2).

Next, an intraperitoneal glucose tolerance test (IPGTT) was performed with a glucose dose of 1.5 g kg^{-1} at 4 h post-administration to assess blood glucose regulation capacity. As shown in Fig. 3d,e, the PGLs in healthy mice and diabetic mice treated with the GR-MN patch returned to normoglycaemia after a blood glucose peak, while the mice treated with the CR-MN patch showed a gradual increase in glucose levels over 120 min. The glucose responsiveness of GR-MN to glucose challenge can also be tuned by adjusting the ratio of DMAEA to 3APBA (Supplementary Fig. 7). It was also possible to adjust the insulin dose using patches of different sizes, to change the response capability to glucose challenge (Supplementary Fig. 8), indicating that this device holds the potential to be personalized during further clinical trials to fit the needs of each person depending on their weight and sensitivity to insulin.

To confirm the blood glucose-promoted insulin release in vivo, a glucose challenge with a higher dose (3 g kg^{-1}) was conducted in diabetic mice at 4 h post-administration of the GR-MN patch. An obvious spike in plasma insulin levels was observed following the increased glucose levels, indicating that the GR-MN patch has rapid glucose responsiveness (Fig. 3f). The haematoxylin

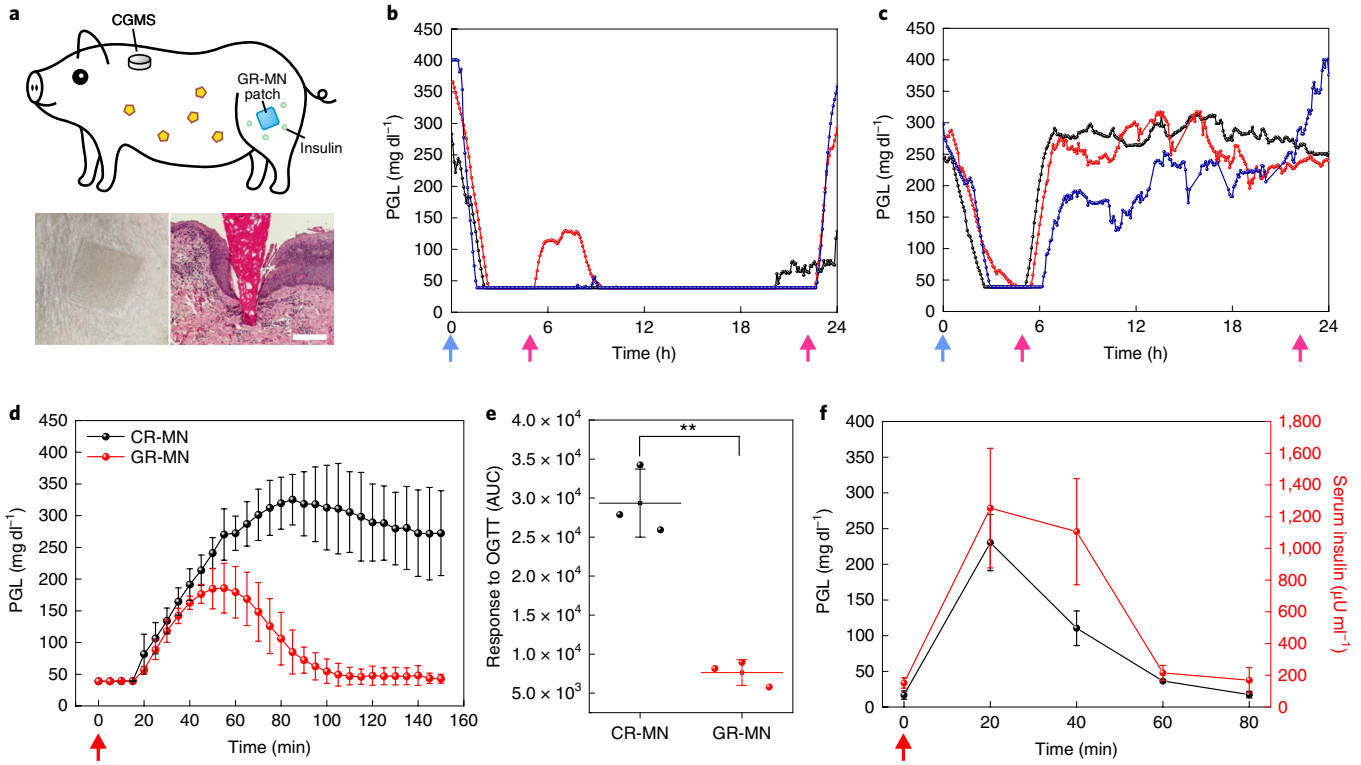

Fig. 4 | In vivo evaluation of GR-MN in an STZ-induced diabetic minipig model. a, Top: schematic of a minipig treated with GR-MN at the leg site and monitored with a CGMS. Bottom left: photograph of a GR-MN patch applied on a minipig's leg. Bottom right: haematoxylin and eosin-stained section of minipig skin penetrated by one microneedle. Scale bar, 200 μm. **b**,**c**, PGLs in STZ-induced diabetic minipigs ($n=3$) after treatment with GR-MN (**b**) and CR-MN (**c**). Insulin dose: 7 mg. **d**, In vivo oral glucose tolerance test in diabetic minipigs ($n=3$) at 4 h post-administration of GR-MN or CR-MN. Glucose dose: 1 g kg^{-1}. **e**, Responsiveness in diabetic minipigs ($n=3$) was calculated based on the AUC from 0–150 min, with the baseline set at the 0-min plasma glucose reading. Statistical significance was determined by two-tailed Student's *t*-test (**$P=1.27\times10^{-3}$). OGTT, oral glucose tolerance test. **f**, In vivo glucose-responsive insulin release promoted by intravenous glucose challenge at 4 h post-administration of the GR-MN patches in diabetic minipigs ($n=3$). Glucose dose: 0.7 g kg^{-1}. The detection range of CGMS was 40–400 mg dl^{-1}. In **b**,**c**, the blue arrows indicate the time points of microneedle administration and the pink arrows indicate the time points of feeding. In **d**,**f**, the red arrows indicate the time points of glucose administration. In **d**–**f**, data are presented as mean ± s.d.

and eosin staining results showed insignificant neutrophil infiltration at the GR-MN-treated site 1 week after administration (Supplementary Fig. 9).

In vivo studies in an STZ-induced diabetic minipig model

The porcine skin is considered a good model for human skin in terms of its general structure, thickness, hair sparseness, and collagen and lipid composition[35]. We therefore further evaluated the in vivo performance of the GR-MN with a 1:4 ratio of DMAEA to 3ABPA in an STZ-induced insulin-deficient Göttingen minipig model. Diabetic minipigs were transcutaneously treated with CR-MN or GR-MN (with an insulin dose of 7 mg) under anaesthesia. As shown in Fig. 4a, the microneedle patch could effectively penetrate the skin of the minipig. To achieve a real-time and sustained record of the minipig glucose levels, a continuous glucose monitoring system (CGMS; Dexcom) was integrated into the minipig experiments. PGLs in both CR-MN- and GR-MN-treated pigs decreased to normoglycaemia after 2 h (Fig. 4b,c). After the afternoon meal, levels in the CR-MN-treated pig immediately increased to a hyperglycaemic state. However, the glucose levels in pigs treated with GR-MN showed a small increase and quickly returned to the normal glycaemic state after the mealtime. The glucose levels could be maintained at a reduced state overnight until the next meal on the second day. During the entire treatment, the pigs were monitored carefully by taking blood samples (Supplementary Table 3). The normal blood glucose range of healthy Göttingen minipigs is 40–80 mg dl^{-1} (Supplementary Fig. 10)[36–40]. Although the glucose levels decreased to <40 mg dl^{-1} (the lower limit of detection of the CGMS) during administration, no symptoms of hypoglycaemia were observed. Furthermore, a study of long-term consecutive administration of GR-MN indicated that blood glucose levels can be well controlled within the normal range for 48 h in both diabetic mice and pigs (Supplementary Fig. 11).

We further performed an oral glucose tolerance test 4 h post-treatment with the CR-MN and GR-MN patches. Similar to the results in the mouse model, glucose levels quickly increased to a hyperglycaemic state after the glucose challenge in the minipig treated with the CR-MN patches (Fig. 4d,e). In contrast, the administered GR-MN patch was able to inhibit the increase of glucose levels after the glucose challenge and to re-establish normoglycaemia after 100 min. An intravenous glucose tolerance test (IVGTT) was conducted to confirm the in vivo glucose-dependent insulin release. As shown in Fig. 4f, the infused dextrose solution led to an immediate increase in glucose levels within the first 20 min, which promoted insulin release into the blood, as verified by the ELISA results. During the IVGTT, concurrent measurements of porcine C-peptide levels showed that endogenous pig insulin was negligible during the experiment (Supplementary Fig. 12). In addition, a second IVGTT was performed when the glucose levels returned to normoglycaemia, and the results also showed an increase in serum insulin levels with the increase of glucose levels (Supplementary Fig. 13), indicating that the GR-MN patch

could achieve continuous glucose responsiveness. After treatment, the GR-MN patch was removed completely from the skin, as confirmed by scanning electron microscopy, with only insignificant fragments found in the skin tissue (Supplementary Fig. 14). Histological images using haematoxylin and eosin staining indicated that limited inflammation occurred after microneedle administration (Supplementary Fig. 15).

Discussion

Integration of glucose-responsive formulations together with microneedle-based transdermal insulin technology[41–43] holds great promise for improved regulation of glucose levels[4,44]. Nonetheless, only few glucose-responsive insulin-delivery formulations have been reported using large animal models of diabetes[45]. For transdermal delivery strategies, one bottleneck for the translation of such an insulin patch involves the limited loading capacity of insulin for clinical usage[46]. To this end, we developed this glucose-responsive insulin patch with an entire polymeric matrix consisting of PBA groups as the glucose-responsive moiety, instead of embedding glucose-responsive formulations such as nanoparticles inside. This microneedle fabrication process based on an in situ photopolymerization strategy is facile and efficient while avoiding the use of extra organic solvents and elevated temperatures to maintain the bioactivity of insulin. In addition, a high encapsulation efficiency of insulin with a high loading capability allows this system to achieve the clinical target dose, unlike previous insulin-loaded microneedle formulations[8,9]. In vivo studies confirmed that the bioactivity of insulin loaded within the patches could be maintained at room temperature for over 8 weeks.

The ratio of the positively charged unit (DMAEA) to the negatively charged unit (3APBA) was adjusted to give an optimized product that possesses a remarkable glucose-dependent insulin release profile. In vivo experiments in STZ-induced diabetic mice showed that GR-MN patches offer glucose-responsive regulation of glucose levels for a prolonged period of time, with a reduced risk of hypoglycaemia. The IPGTT results indicated that a glucose challenge could trigger the fast release of insulin by the GR-MN patch. The patch can also be personalized by adjusting the ratio of DMAEA to 3APBA, or the size, to fit the needs of individuals with different weights and sensitivities to insulin. Based on the encouraging results in the diabetic mouse model, a series of studies were further conducted on diabetic minipigs. This showed that the GR-MN patch was able to maintain minipig glucose levels in a nearly normal range for over 20 h under normal feeding conditions. Oral administration of dextrose solution as a simulation of feeding indicated that the GR-MN patch could achieve enhanced regulation of glucose levels back to the normal range compared with the CR-MN patch. Increased glucose levels caused by intravenous infusion of dextrose solution promoted significant insulin release from the GR-MN patch. Furthermore, the repeated IVGTTs showed that the GR-MN patch had the capability to rapidly respond to the changes in glucose levels for multiple rounds of glucose challenges.

Since the crosslinked polymeric matrix of the GR-MN patch is non-degradable, it can be completely removed from the skin after treatment. Unlike the dissolvable microneedle, which may raise safety concerns associated with the foreign body response to deposited needle tip materials, the well-designed GR-MN patch revealed good biocompatibility with skin tissues. Furthermore, the avoidance of glucose oxidase as the glucose-responsive moiety in this system can prevent generation of the toxic by-product hydrogen peroxide, improving its safety with long-term use[47]. The GR-MN patch developed in this study also provides a technology for the development of stimuli-responsive transdermal delivery systems for other drugs, including insulin analogues[19,48], glucagon-like peptide-1 receptor agonist[49] and glucagon[50].

Methods

Materials. All of the chemicals were purchased from Sigma–Aldrich unless otherwise specified and were used as received. Norland Optical Adhesive was purchased from Norland Products. 3APBA was purchased from Boron Molecular. Human recombinant insulin was purchased from Thermo Fisher Scientific (catalogue number A11382IJ). The deionized water was prepared using a Millipore NANOPure purification system (resistivity > 18.2 MΩ cm^{-1}).

GR-MN and non-responsive CR-MN preparation. The GR-MN patch was prepared by in situ polymerization under ultraviolet irradiation. Monomers with photoinitiator were first prepared by dissolving DMAEA and 3APBA at a certain ratio in NVP containing EGDMA (0.5 mol%) as the crosslinker and Irgacure 2959 (1 mol%) as the photoinitiator. After this, insulin was dispersed in the prepared monomer solution (20 wt%) and the solution was directly deposited by pipette onto the microneedle mould surface. Moulds were then placed under vacuum for 10 min to allow the liquid to fill the microneedle mould. After removing the excess solution, the mould was placed under an ultraviolet lamp (100 W; 365 nm; Blak-Ray) for 20 min at 4 °C. Afterwards, the ultraviolet-curable base material (Norland Optical Adhesive) was added onto the mould and further cured under ultraviolet light for 10 min to form the base of the patch. The resulting patches were carefully separated from the mould and immersed in PBS/ethanol mixtures (80:20; *v*/*v*) for 2 h to remove the unreacted monomers. The patch was dried in a vacuum desiccator after purification and stored in a sealed six-well container at room temperature for further study. The CR-MN patch was prepared in a similar way, but without adding DMAEA and 3APBA.

Mechanical strength test. The mechanical strength of the microneedles was measured by pressing them against a stainless-steel plate. The initial gauge was set to 2.00 mm between the microneedle tips and the stainless-steel plate, with 10.00 N as the load cell capacity. The speed of the top stainless-steel plate movement towards the microneedles was 0.1 mm min^{-1}. The failure force of the microneedles was recorded when the needles began to buckle.

Analysis of leachable monomers. To measure the amounts of leachable monomers for the purified microneedles, the purified patch was incubated in 2 ml PBS (137 mM NaCl, 2.7 mM KCl, 10 mM Na_2HPO_4 and 2 mM KH_2PO_4 (pH 7.4)) at 37 °C for 24 h. Analysis of the released monomers was carried out by HPLC with a Photodiode Array Detectors detector (200–600 nm) using a Varian Pursuit 3 PFP 50 mm × 2.0 mm column (for the analysis of NVP, 3APBA and EGDMA) and a Waters C18 reverse 250 mm × 4.6 mm column (for the analysis of DMAEA). Gradient HPLC methods (represented in Supplementary Tables 4 and 5) were developed and used for the analysis of each monomer. All of the measurements were performed three times for each of the extracts. Standard solutions of NVP, 3APBA, DMAEA and EGDMA were prepared by dissolving each monomer in varied concentrations.

Mass spectrum analysis. Insulin was extracted from the prepared GR-MN patches in 0.01 M HCl at 4 °C for 24 h. The spectra of the extracted insulin and native insulin were detected using a Waters ACQUITY LC-MS system using a Varian Pursuit 3 PFP 50 mm × 2.0 mm column and analysed by MassLynx.

In vitro glucose binding study. The samples were incubated in 1 ml PBS with various glucose concentrations (50, 100 and 400 mg dl^{-1}) at 37 °C for 4 h. After removal of the samples, the remaining glucose in the solution was measured using a Clarity GL2PLUS glucose meter (Clarity Diagnostics). The concentration was calibrated using a glucose standard curve.

In vitro release studies. To evaluate the glucose responsiveness of the glucose-responsive matrix, the samples were incubated in 1 ml PBS with various glucose concentrations (0, 100 and 400 mg dl^{-1}) at 37 °C. At predetermined time points, 50 µl of the medium was removed and the released amount of insulin was examined using a Coomassie Plus protein assay. The absorbance was detected at 595 nm on the Infinite 200 PRO multimode plate reader (Tecan Group), and the insulin content was calibrated with an insulin standard curve. To test the ability to adapt to cyclical changes in glucose levels, the sample was first incubated in PBS with 100 mg dl^{-1} glucose for 30 min. At that point, the sample was removed and subsequently incubated in PBS with 400 mg dl^{-1} glucose for another 30 min. This cycle was repeated several times. The released insulin was measured using the same method as described above.

In vivo studies using STZ-induced diabetic mice. The in vivo efficacy of glucose-responsive insulin patches for diabetes treatment was evaluated on STZ-induced adult diabetic mice (male C57BL/6J mice; 6–8 weeks of age; The Jackson Laboratory). The animal study protocol was approved by the Institutional Animal Care and Use Committee at North Carolina State University, the University of North Carolina at Chapel Hill and the University of California, Los Angeles. The plasma-equivalent glucose was measured from tail vein blood samples (~3 µl) of mice using the Clarity GL2PLUS glucose meter. The patches used for the mice had an 11 × 11 array of microneedles of pyramidal shape, with a width of 300 µm

at the base and a height of 700 μm. Five mice from each group were selected for transcutaneous treatment with CR-MN or GR-MN patches loaded with human recombinant insulin (insulin dose: 0.5 mg). To measure the RBA of the patch, five mice were treated with subcutaneous injection of human recombinant insulin (insulin dose: 0.05 mg) The glucose levels of each mouse were monitored over time. To measure the plasma insulin concentration in vivo, 25 μl blood was drawn from the tail vein of mice at the indicated time points. The plasma was isolated and stored at −20 °C until it was assayed. The plasma insulin concentration was measured using a Human Insulin ELISA kit according to the manufacturer's protocol (Invitrogen). The RBA was calculated using the equation:

$$\mathrm{RBA}(\%) = (\mathrm{AUC}_{\mathrm{MN}} \times \mathrm{dose}_{\mathrm{SC}})/(\mathrm{AUC}_{\mathrm{SC}} \times \mathrm{dose}_{\mathrm{MN}}) \times 100$$

where $\mathrm{AUC}_{\mathrm{MN}}$ is the area under the curve after applying the GR-MN or CR-MN patches, and $\mathrm{AUC}_{\mathrm{SC}}$ indicates the area under the curve after subcutaneous injection of insulin.

To assess the efficacy of long-term consecutive administration of the GR-MN patches, five diabetic mice were transcutaneously treated with the GR-MN patches loaded with human recombinant insulin (insulin dose: 0.5 mg). The patches were replaced every 12 h within the same skin area. Glucose levels of each mouse were monitored over time.

An intraperitoneal glucose tolerance test was conducted to confirm the in vivo glucose responsiveness of microneedles 4 h after the administration of the CR-MN or GR-MN patches. Briefly, mice were administrated with the CR-MN or GR-MN patches, then a glucose solution in PBS was injected intraperitoneally into all mice at a dose of 1.5 g kg^{-1}. The glucose levels were monitored over time after injection. The glucose tolerance test on healthy mice was used as a control. To verify that the in vivo IPGTT promoted insulin release, a high glucose dose (3 g kg^{-1}) was given 4 h after administration of the GR-MN patches. Glucose levels were monitored and 25 μl of blood was drawn from the tail vein of mice at the indicated time points. Plasma was isolated and stored at −20 °C until it was assayed. The plasma insulin concentration was measured using a Human Insulin ELISA kit (Mercodia).

In vivo studies using STZ-induced diabetic minipigs. The animal study protocol was approved by the Institutional Animal Care and Use Committee at North Carolina State University, the University of North Carolina at Chapel Hill and the University of California, Los Angeles. Three male Göttingen minipigs (Marshall BioResources) aged 6 months at arrival were used. Diabetes was induced in the minipigs by means of STZ infusion (150 mg kg^{-1}). STZ was dissolved in freshly prepared disodium citrate buffer (pH 4.5) at a concentration of 75 mg ml^{-1} and administered intravenously within 10 min. After 7 d of recovery, successful establishment of the insulin-deficient diabetes model was confirmed by monitoring the glucose levels using the CGMS (Dexcom G4 Platinum Continuous Glucose Monitor; Dexcom). The diabetic minipigs were treated with insulin glargine (0.3–0.8 U kg^{-1}; Lantus; Sanofi-Aventis) once daily for glucose control, and the daily treatment was stopped 36 h before the experiment to minimize the impact of remaining insulin glargine. All minipigs (weight: ~25–30 kg) were fasted overnight before administration. The minipigs were treated transcutaneously with the CR-MN or GR-MN patches at the leg sites at an insulin dose of 7 mg for each pig at 10:00. The patches used for minipigs had a 20 × 20 array of microneedles of pyramidal shape, with a width of 400 μm at the base and a height of 900 μm. To fix the patch on the skin surface, 3 M Tegaderm transparent film dressing was used to cover the patch. PGLs were continuously monitored using CGMS, and two daily meals were provided during the experiment. The CGMS was calibrated according to the manufacturer's manual during the experiment by measuring the plasma glucose using a Clarity GL2PLUS glucose meter.

To assess the efficacy of long-term consecutive administration of the GR-MN patches, three diabetic minipigs were treated transcutaneously with GR-MN patches loaded with human recombinant insulin (insulin dose: 7 mg). The patches were replaced every 24 h within the same skin area. The glucose levels were continuously monitored with the CGMS, and two daily meals were provided during the experiment.

An oral glucose tolerance test was conducted on diabetic minipigs to assess the glucose responsiveness of the microneedle patches. All minipigs were fasted overnight before administration. The minipigs were transcutaneously treated with the CR-MN or CR-MN patches at the leg site at an insulin dose of 7 mg per pig at 10:00. A glucose solution was administered orally to the minipigs 4 h post-treatment at a dose of 1 g kg^{-1}. The PGLs were continuously monitored using the CGMS.

An IVGTT was further performed to confirm the blood glucose-promoted insulin release from the microneedles. Three diabetic pigs were treated transcutaneously at 10:00 with the GR-MN patches after overnight fasting. Dextrose solution (5 wt%) was intravenously infused into pigs at a rate of 1 l h^{-1} at 4 h post-treatment at a dose of 0.7 g kg^{-1}. Blood was collected from the jugular vein at the indicated time points for measurement of plasma glucose using a Clarity GL2PLUS glucose meter, and the serum was then separated using Serum Separator Tubes (BD Vacutainer). Serum insulin levels were determined using a Human Insulin ELISA kit, and porcine C-peptide levels were measured using a Porcine C-peptide ELISA kit, according to the manufacturer's protocol (Mercodia).

Statistics. All of the results are presented as means ± s.d. Statistical analysis was performed using a two-tailed Student's *t*-test. The differences between experimental groups and control groups were considered statistically significant at $P < 0.05$.

Reporting Summary. Further information on research design is available in the Nature Research Reporting Summary linked to this article.

Data availability

The authors declare that all of the data supporting the findings of this study are available within the paper and the Supplementary Information.

Received: 12 June 2019; Accepted: 10 December 2019;
Published online: 3 February 2020

References

1. Veiseh, O., Tang, B. C., Whitehead, K. A., Anderson, D. G. & Langer, R. Managing diabetes with nanomedicine: challenges and opportunities. *Nat. Rev. Drug Discov.* **14**, 45–57 (2015).
2. Ohkubo, Y. et al. Intensive insulin therapy prevents the progression of diabetic microvascular complications in Japanese patients with non-insulin-dependent diabetes mellitus: a randomized prospective 6-year study. *Diabetes Res. Clin. Pract.* **28**, 103–117 (1995).
3. Owens, D. R., Zinman, B. & Bolli, G. B. Insulins today and beyond. *Lancet* **358**, 739–746 (2001).
4. Bakh, N. A. et al. Glucose-responsive insulin by molecular and physical design. *Nat. Chem.* **9**, 937–943 (2017).
5. Yu, J., Zhang, Y., Bomba, H. & Gu, Z. Stimuli-responsive delivery of therapeutics for diabetes treatment. *Bioeng. Transl. Med.* **1**, 323–337 (2016).
6. Ravaine, V., Ancla, C. & Catargi, B. Chemically controlled closed-loop insulin delivery. *J. Control. Release* **132**, 2–11 (2008).
7. Wu, Q., Wang, L., Yu, H., Wang, J. & Chen, Z. Organization of glucose-responsive systems and their properties. *Chem. Rev.* **111**, 7855–7875 (2011).
8. Yu, J. et al. Microneedle-array patches loaded with hypoxia-sensitive vesicles provide fast glucose-responsive insulin delivery. *Proc. Natl Acad. Sci. USA* **112**, 8260–8265 (2015).
9. Yu, J. et al. Hypoxia and H_2O_2 dual-sensitive vesicles for enhanced glucose-responsive insulin delivery. *Nano Lett.* **17**, 733–739 (2017).
10. Kost, J., Leong, K. & Langer, R. Ultrasound-enhanced polymer degradation and release of incorporated substances. *Proc. Natl Acad. Sci. USA* **86**, 7663–7666 (1989).
11. Podual, K., Doyle, F. J. III & Peppas, N. A. Glucose-sensitivity of glucose oxidase-containing cationic copolymer hydrogels having poly (ethylene glycol) grafts. *J. Control. Release* **67**, 9–17 (2000).
12. Podual, K., Doyle Iii, F. & Peppas, N. Preparation and dynamic response of cationic copolymer hydrogels containing glucose oxidase. *Polymer* **41**, 3975–3983 (2000).
13. Gu, Z. et al. Injectable nano-network for glucose-mediated insulin delivery. *ACS Nano* **7**, 4194–4201 (2013).
14. Brownlee, M. & Cerami, A. A glucose-controlled insulin-delivery system: semisynthetic insulin bound to lectin. *Science* **206**, 1190–1191 (1979).
15. Brownlee, M. & Cerami, A. Glycosylated insulin complexed to concanavalin A: biochemical basis for a closed-loop insulin delivery system. *Diabetes* **32**, 499–504 (1983).
16. Wang, C. et al. Red blood cells for glucose-responsive insulin delivery. *Adv. Mater.* **29**, 1606617 (2017).
17. Yang, R. et al. A glucose-responsive insulin therapy protects animals against hypoglycemia. *JCI Insight* **3**, 97476 (2018).
18. Wang, J. et al. Charge-switchable polymeric complex for glucose-responsive insulin delivery in mice and pigs. *Sci. Adv.* **5**, eaaw4357 (2019).
19. Chou, D. H.-C. et al. Glucose-responsive insulin activity by covalent modification with aliphatic phenylboronic acid conjugates. *Proc. Natl Acad. Sci. USA* **112**, 2401–2406 (2015).
20. Matsumoto, A. et al. Synthetic "smart gel" provides glucose-responsive insulin delivery in diabetic mice. *Sci. Adv.* **3**, eaaq0723 (2017).
21. Matsumoto, A., Yoshida, R. & Kataoka, K. Glucose-responsive polymer gel bearing phenylborate derivative as a glucose-sensing moiety operating at the physiological pH. *Biomacromolecules* **5**, 1038–1045 (2004).
22. Kataoka, K., Miyazaki, H., Bunya, M., Okano, T. & Sakurai, Y. Totally synthetic polymer gels responding to external glucose concentration: their preparation and application to on–off regulation of insulin release. *J. Am. Chem. Soc.* **120**, 12694–12695 (1998).
23. Matsumoto, A. et al. A synthetic approach toward a self-regulated insulin delivery system. *Angew. Chem. Int. Ed.* **51**, 2124–2128 (2012).
24. Mo, R., Jiang, T., Di, J., Tai, W. & Gu, Z. Emerging micro- and nanotechnology based synthetic approaches for insulin delivery. *Chem. Soc. Rev.* **43**, 3595–3629 (2014).

25. Ye, T. et al. Tailoring the glucose-responsive volume phase transition behaviour of Ag@poly(phenylboronic acid) hybrid microgels: from monotonous swelling to monotonous shrinking upon adding glucose at physiological pH. *Polym. Chem.* **5**, 2352–2362 (2014).
26. Wu, W., Mitra, N., Yan, E. C. & Zhou, S. Multifunctional hybrid nanogel for integration of optical glucose sensing and self-regulated insulin release at physiological pH. *ACS Nano* **4**, 4831–4839 (2010).
27. Wu, X. et al. Selective sensing of saccharides using simple boronic acids and their aggregates. *Chem. Soc. Rev.* **42**, 8032–8048 (2013).
28. Brooks, W. L. & Sumerlin, B. S. Synthesis and applications of boronic acid-containing polymers: from materials to medicine. *Chem. Rev.* **116**, 1375–1397 (2015).
29. Sullivan, S. P. et al. Dissolving polymer microneedle patches for influenza vaccination. *Nat. Med.* **16**, 915–920 (2010).
30. Sullivan, S. P., Murthy, N. & Prausnitz, M. R. Minimally invasive protein delivery with rapidly dissolving polymer microneedles. *Adv. Mater.* **20**, 933–938 (2008).
31. Prausnitz, M. R. Microneedles for transdermal drug delivery. *Adv. Drug Deliv. Rev.* **56**, 581–587 (2004).
32. Vancoillie, G. & Hoogenboom, R. Synthesis and polymerization of boronic acid containing monomers. *Polym. Chem.* **7**, 5484–5495 (2016).
33. Ding, Z., Guan, Y., Zhang, Y. & Zhu, X. Layer-by-layer multilayer films linked with reversible boronate ester bonds with glucose-sensitivity under physiological conditions. *Soft Matter* **5**, 2302–2309 (2009).
34. Hisamitsu, I., Kataoka, K., Okano, T. & Sakurai, Y. Glucose-responsive gel from phenylborate polymer and poly(vinyl alcohol): prompt response at physiological pH through the interaction of borate with amino group in the gel. *Pharm. Res.* **14**, 289–293 (1997).
35. Summerfield, A., Meurens, F. & Ricklin, M. E. The immunology of the porcine skin and its value as a model for human skin. *Mol. Immunol.* **66**, 14–21 (2015).
36. Larsen, M. O. et al. Mild streptozotocin diabetes in the Göttingen minipig. A novel model of moderate insulin deficiency and diabetes. *Am. J. Physiol. Endocrinol. Metab.* **282**, E1342–E1351 (2002).
37. Larsen, M. O., Rolin, B., Wilken, M., Carr, R. D. & Gotfredsen, C. F. Measurements of insulin secretory capacity and glucose tolerance to predict pancreatic β-cell mass in vivo in the nicotinamide/streptozotocin Göttingen minipig, a model of moderate insulin deficiency and diabetes. *Diabetes* **52**, 118–123 (2003).
38. Akhtar, M. S., Ramzan, A., Ali, A. & Ahmad, M. Effect of Amla fruit (*Emblica officinalis* Gaertn.) on blood glucose and lipid profile of normal subjects and type 2 diabetic patients. *Int. J. Food Sci. Nutr.* **62**, 609–616 (2011).
39. Larsen, M. O. & Rolin, B. Use of the Göttingen minipig as a model of diabetes, with special focus on type 1 diabetes research. *ILAR J.* **45**, 303–313 (2004).
40. Larsen, M. et al. The conscious Göttingen minipig as a model for studying rapid pulsatile insulin secretion in vivo. *Diabetologia* **45**, 1389–1396 (2002).
41. Prausnitz, M. R. & Langer, R. Transdermal drug delivery. *Nat. Biotechnol.* **26**, 1261–1268 (2008).
42. Zhang, Y. et al. Advances in transdermal insulin delivery. *Adv. Drug Deliv. Rev.* **139**, 51–70 (2018).
43. Yu, J., Zhang, Y., Kahkoska, A. R. & Gu, Z. Bioresponsive transcutaneous patches. *Curr. Opin. Biotechnol.* **48**, 28–32 (2017).
44. Lu, Y., Aimetti, A. A., Langer, R. & Gu, Z. Bioresponsive materials. *Nat. Rev. Mater.* **2**, 16075 (2017).
45. Kaarsholm, N. C. et al. Engineering glucose responsiveness into insulin. *Diabetes* **67**, 299–308 (2018).
46. Yang, S. et al. Phase-transition microneedle patches for efficient and accurate transdermal delivery of insulin. *Adv. Funct. Mater.* **25**, 4633–4641 (2015).
47. Gu, Z. & Wang, J. Charge-switchable polymeric depot for glucose-triggered insulin delivery with ultrafast response. Patent no. WO2019104006A1 (2017).
48. Wang, J. et al. Glucose transporter inhibitor-conjugated insulin mitigates hypoglycemia. *Proc. Natl Acad. Sci. USA* **116**, 10744–10748 (2019).
49. Chen, W. et al. Microneedle-array patches loaded with dual mineralized protein/peptide particles for type 2 diabetes therapy. *Nat. Commun.* **8**, 1777 (2017).
50. Yu, J. et al. Insulin-responsive glucagon delivery for prevention of hypoglycemia. *Small* **13**, 1603028 (2017).

Acknowledgements

This work was supported by grants from Zenomics Inc. and a start-up package from University of California, Los Angeles. We acknowledge the use of the Analytical Instrumentation Facility at North Carolina State, which is supported by the State of North Carolina and National Science Foundation. A.R.K. is supported by the National Institute of Diabetes and Digestive and Kidney Diseases of the National Institutes of Health (grant no. F30DK113728). The content is solely the responsibility of the authors and does not necessarily represent the official views of the National Institutes of Health.

Author contributions

J.Y. and Z.G. conceived the study idea. J.Y., A.R.K., J.B.B., R.L. and Z.G. designed the experiments. J.Y., J.W., Y.Z., G.C., W.M. and Y.Y. performed the experiments. All authors contributed to writing the manuscript, discussing the results and implications and editing the manuscript at all stages.

Competing interests

Z.G., J.Y. and G.C. have applied for patents related to this study. Z.G. is a scientific co-founder of Zenomics Inc. R.L. and J.B.B. are Scientific Advisory Board members of Zenomics Inc. J.Y., Y.Z., W.M. and Y.Y. are full-time employees of Zenomics Inc. R.L. discloses potential competing interests due to his affiliation with Zenomics Inc. For a list of entities with which R.L. is involved, compensated or uncompensated, see https://tinyurl.com/RLCOINBME. The remaining authors declare no competing interests.

Additional information

Supplementary information is available for this paper at https://doi.org/10.1038/s41551-019-0508-y.

Correspondence and requests for materials should be addressed to Z.G.

Reprints and permissions information is available at www.nature.com/reprints.

Publisher's note Springer Nature remains neutral with regard to jurisdictional claims in published maps and institutional affiliations.

nature research

Corresponding author(s): Zhen Gu

Last updated by author(s): Nov 27, 2019

Reporting Summary

Nature Research wishes to improve the reproducibility of the work that we publish. This form provides structure for consistency and transparency in reporting. For further information on Nature Research policies, see Authors & Referees and the Editorial Policy Checklist.

Statistics

For all statistical analyses, confirm that the following items are present in the figure legend, table legend, main text, or Methods section.

n/a	Confirmed	
☐	☒	The exact sample size (*n*) for each experimental group/condition, given as a discrete number and unit of measurement
☐	☒	A statement on whether measurements were taken from distinct samples or whether the same sample was measured repeatedly
☐	☒	The statistical test(s) used AND whether they are one- or two-sided *Only common tests should be described solely by name; describe more complex techniques in the Methods section.*
☒	☐	A description of all covariates tested
☐	☒	A description of any assumptions or corrections, such as tests of normality and adjustment for multiple comparisons
☐	☒	A full description of the statistical parameters including central tendency (e.g. means) or other basic estimates (e.g. regression coefficient) AND variation (e.g. standard deviation) or associated estimates of uncertainty (e.g. confidence intervals)
☐	☒	For null hypothesis testing, the test statistic (e.g. *F*, *t*, *r*) with confidence intervals, effect sizes, degrees of freedom and *P* value noted *Give P values as exact values whenever suitable.*
☒	☐	For Bayesian analysis, information on the choice of priors and Markov chain Monte Carlo settings
☒	☐	For hierarchical and complex designs, identification of the appropriate level for tests and full reporting of outcomes
☒	☐	Estimates of effect sizes (e.g. Cohen's *d*, Pearson's *r*), indicating how they were calculated

Our web collection on statistics for biologists contains articles on many of the points above.

Software and code

Policy information about availability of computer code

Data collection	Fluorescent imaging was collected on Zeiss 710.
Data analysis	Statistical analyses were performed by using Microsoft Excel 2016 for Windows 10 and OriginPro 2018. ImageJ (Version 1.52a) was used for fluorescence-image analysis.

For manuscripts utilizing custom algorithms or software that are central to the research but not yet described in published literature, software must be made available to editors/reviewers. We strongly encourage code deposition in a community repository (e.g. GitHub). See the Nature Research guidelines for submitting code & software for further information.

Data

Policy information about availability of data

All manuscripts must include a data availability statement. This statement should provide the following information, where applicable:

- Accession codes, unique identifiers, or web links for publicly available datasets
- A list of figures that have associated raw data
- A description of any restrictions on data availability

The authors declare that all data supporting the findings of this study are available within the paper and its Supplementary Information.

Field-specific reporting

Please select the one below that is the best fit for your research. If you are not sure, read the appropriate sections before making your selection.

☒ Life sciences ☐ Behavioural & social sciences ☐ Ecological, evolutionary & environmental sciences

Life sciences study design

All studies must disclose on these points even when the disclosure is negative.

Sample size	The sample size were determined as per the pilot study or previous experimental experience.
Data exclusions	No data were excluded.
Replication	The experimental findings were reliably reproduced.
Randomization	All samples/organisms were randomly allocated into experimental groups.
Blinding	No formal blinding was used.

Reporting for specific materials, systems and methods

We require information from authors about some types of materials, experimental systems and methods used in many studies. Here, indicate whether each material, system or method listed is relevant to your study. If you are not sure if a list item applies to your research, read the appropriate section before selecting a response.

Materials & experimental systems

n/a	Involved in the study
☒	☐ Antibodies
☒	☐ Eukaryotic cell lines
☒	☐ Palaeontology
☐	☒ Animals and other organisms
☒	☐ Human research participants
☒	☐ Clinical data

Methods

n/a	Involved in the study
☒	☐ ChIP-seq
☒	☐ Flow cytometry
☒	☐ MRI-based neuroimaging

Animals and other organisms

Policy information about studies involving animals; ARRIVE guidelines recommended for reporting animal research

Laboratory animals	Male C57BL/6J streptozotocin-induced diabetic mice (six-to-eight weeks) were purchased from Jackson Lab. Male Gottingen minipigs (six months) were purchased from Marshall BioResources.
Wild animals	The study did not involve wild animals.
Field-collected samples	The study did not involve samples collected from the field.
Ethics oversight	All the animal studies strictly followed the animal protocol approved by the Institutional Animal Care and Use Committee at the University of North Carolina at Chapel Hill and North Carolina State University, and University of California, Los Angeles.

Note that full information on the approval of the study protocol must also be provided in the manuscript.